NANO LETTERS

Letter

Cite This: Nano Lett. 2019, 19, 7078−7084

pubs.acs.org/NanoLett

Photon Correlation Spectroscopy of Luminescent Quantum Defects in Carbon Nanotubes

Manuel Nutz,[†,‡] Jiaxiang Zhang,[†,§] Mijin Kim,[∥] Hyejin Kwon,[∥] Xiaojian Wu,[∥] YuHuang Wang,[∥] and Alexander Högele*[,†,‡]

[†]Faculty of Physics, Munich Quantum Center and Center for NanoScience (CeNS), Ludwig-Maximilians-Universität München, Geschwister-Scholl-Platz 1, 80539 München, Germany

[‡]Munich Center for Quantum Science and Technology (MCQST), Schellingtr. 4, 80799 München, Germany

[∥]Department of Chemistry and Biochemistry, University of Maryland, 8051 Regent Drive, College Park, Maryland 20742, United States

[§]Shanghai Institute of Microsystem and Information Technology, Chinese Academy of Sciences, 865 Changning Road, Shanghai 200050, China

Supporting Information

ABSTRACT: Defect-decorated single-wall carbon nanotubes have shown rapid growing potential for imaging, sensing, and the development of room-temperature single-photon sources. The key to the highly nonclassical emission statistics is the discrete energy spectrum of defect-localized excitons. However, variations in defect configurations give rise to distinct spectral bands that may compromise single-photon efficiency and purity in practical devices, and experimentally it has been challenging to study the exciton population distribution among the various defect-specific states. Here, we performed photon correlation spectroscopy on hexyl-decorated single-wall carbon nanotubes to unravel the dynamics and competition between neutral and charged exciton populations. With autocorrelation measurements at the single-tube level, we prove the nonclassical photon emission statistics of defect-specific exciton and trion photoluminescence and identify their mutual exclusiveness in photoemissive events with cross-correlation spectroscopy. Moreover, our study reveals the presence of a dark state with population-shelving time scales between 10 and 100 ns. These new insights will guide further development of chemically tailored carbon nanotube states for quantum photonics applications.

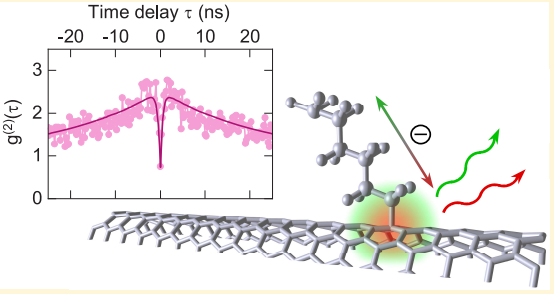

KEYWORDS: *Carbon nanotubes, covalent quantum defects, photoluminescence spectroscopy, photon correlation spectroscopy, single photon emission statistics, bunching, antibunching, localized excitons, localized trions*

Solid-state sources of nonclassical light with controlled quantum correlations in photon emission are indispensable for the development of quantum photonic technologies. In addition to single-photon sources in crystalline bulk such as self-assembled quantum dots[1] and color centers in diamond[2] or hexagonal boron nitride,[3] local defects in atomically thin two-dimensional semiconductors[4−7] and one-dimensional carbon nanotubes (CNTs)[8−11] are known to exhibit highly nonclassical correlations in photon emission statistics. More recently, remarkable control in the creation of nanotube sidewall defects with deep exciton-localizing traps[12−22] has established covalently functionalized CNTs with increased quantum yields[12−14] and room-temperature single-photon emission[16] at telecom wavelengths[20] as a new paradigm system for solid-state quantum photonics.[23,24]

These outstanding aspects of functionalized CNTs with room-temperature, telecom band, high-purity single-photon emission,[20] however, are occasionally compromised by the multiplicity of spectrally distinct photoactive states,[15,18−21] presumably stemming from different charge or bonding configurations of exciton-localizing covalent defects. Improved understanding and control of defect conformations at the atomistic level indicates that the photoluminescence (PL) dispersity can be reduced to favor one emissive defect state,[25] but even optimized structures are not completely void of PL line multiplicity. In CNTs decorated with sp^3-defects that promote localization of both neutral excitons and trions, two respective PL bands with emission energies well below the one-dimensional energy continuum of diffusive E_{11} excitons have been observed at the ensemble level.[22,26] At the level of individual nanotubes, a detailed understanding of the exciton population distribution among these distinct PL states would provide guidelines for further developments of chemically

Received: June 24, 2019
Revised: August 14, 2019
Published: September 3, 2019

DOI: 10.1021/acs.nanolett.9b02553
Nano Lett. 2019, 19, 7078−7084

functionalized CNTs for applications in optical sensing and quantum photonics.

In the present work, we employed photon correlation spectroscopy to study correlations in the PL of two spectrally distinct states of luminescent quantum defects in (6,5)-chiral CNTs modified by covalent attachment of hexyl groups.[17,22] The chemical side-wall treatment gives rise to one or more defects per tube with deep trap potentials characterized by PL bands of neutral excitons (X) and trions (T).[22,26] As covalent CNT chemistry is known to favor proximal defects[27] via defect-assisted local destabilization of the carbon lattice with subsequent formation of a second defect in immediate proximity, the enhanced probability of divalent defect formation[28] is common in functionalized nanotubes. The related PL spectra of defect-decorated CNTs are thus rich in diversity, with frequent peak multiplicity in cryogenic single-tube PL.[17,25,28,29]

In the photoluminescence excitation (PLE) maps of defect-functionalized ensembles at room temperature (RT), the diversity simplifies to inhomogeneously broadened defect-specific emission bands. This is also the case for the hexyl-functionalized (6,5)-nanotubes of our study, as shown in Figure 1a, with E_{11}, X, and T bands centered around 1.26, 1.13, and 1.01 eV. For cryogenic experiments at the single tube level, the CNTs were dispersed out of an aqueous suspension onto the flat side of a hemispherical solid immersion lens (SIL) with an average spatial density of less than one tube per focal spot area of ~1 μm diameter.[8] The sample was cooled to the temperature of liquid helium (4.2 K) and displaced laterally with respect to confocal excitation and detection focal points to identify PL hot-spots with spectra as in Figure 1b. The spectra reflect evident variations in PL peak energy, intensity, and line shape across the sample. In some instances, the cryogenic PL was dominated by a single peak (topmost spectrum in Figure 1b), and other spots featured emission of two peaks with comparable intensities (second spectrum from top in Figure 1b) or multipeak spectra (third spectrum from top in Figure 1b, see also Figure S1 in Section I of the Supporting Information). In most cases, the E_{11} emission was weak and occasionally effected by exciton localization as signified by PL red-shifts up to a few tens of meV[30] or antibunching in the emission statistics[8] (Figure S3 in Section II of the Supporting Information).

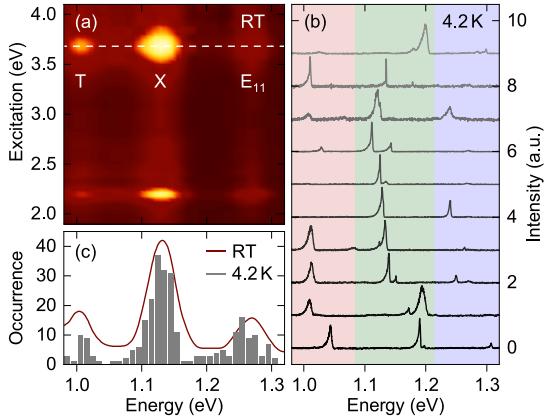

Figure 1. (a) RT PLE map of functionalized CNTs with three characteristic states E_{11}, X, and T with peak emission energies at 1.26, 1.13, and 1.01 eV, respectively. (b) PL spectra of individual functionalized CNTs at 4.2 K (the spectra were offset for clarity; the spectral bands of E_{11}, X, and T emission are shaded in blue, green, and red, respectively). (c) Histogram of emission peak energies of all cryogenic CNTs (gray) compared with the RT ensemble spectrum (wine) obtained from the line-cut indicated by the dashed line in (a).

At the statistical level, and in accord with the RT ensemble characteristics (solid line in Figure 1c), all spectral differences of cryogenic single-tube PL merged into inhomogeneous distributions of E_{11}, X, and T emission bands with a full-width at half-maximum (fwhm) broadening of about 50 meV for all three peaks of the histogram in Figure 1c. The following set of experiments were performed on hot-spots with emission in both X and T spectral bands (shaded in green and red in Figure 1b), occasionally accompanied by E_{11} emission (within the spectral band shaded in blue in Figure 1b), yet without bias to additional peak multiplicity. Taking into account the statistical spatial distribution of CNTs on the sample, our PL experiments thus may probe multiple tubes, multiple defects of an individual tube, or fluctuating configurations of a single defect within the diffraction-limited spot of our cryogenic microscope.

The results of time-resolved PL measurements performed on such local hot-spots with predominant X and T and occasional E_{11} emission are summarized in Figure 2. Biexponential PL dynamics within the E_{11}, X, and T spectral bands are exemplified in Figure 2a for a specific spot. In contrast to this example, the majority of other PL hot-spots were characterized by strictly monoexponential decays. To access the distribution of decay time scales on the statistical level of different measurement hot-spots, we used biexponential fits to the data (solid lines in Figure 2a–c) to extract the characteristic time components τ_1 and τ_2 and their respective fractional contributions to the total PL decay (closed and open circles in Figure 2d–f, respectively). In all cases of monoexponential decay, the weight of one decay channel

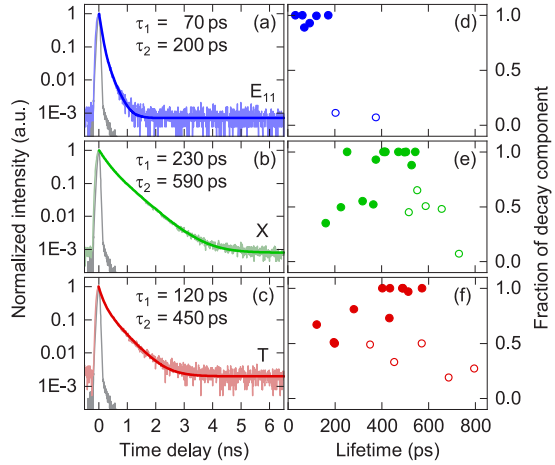

Figure 2. (a–c) Time-resolved PL decay at 4.2 K for the E_{11} (blue), X (green), and T (red) emission from a single CNT with biexponential decay characteristics. The excitation was carried out via photon sidebands of E_{11} in the range 833–920 nm with 1–20 μW laser power; the instrument response function is shown in gray. Two characteristic lifetimes, τ_1 and τ_2, were determined from biexponential fits (solid lines) to the data. (d–f) Fraction of the total PL decay associated with the decay channel characterized by τ_1 (closed circles) and τ_2 (open circles). Note that the majority of the CNTs of our cryogenic study exhibited monoexponential decays, which explains the difference in the number of closed and open symbols.

DOI: 10.1021/acs.nanolett.9b02553
Nano Lett. 2019, 19, 7078–7084

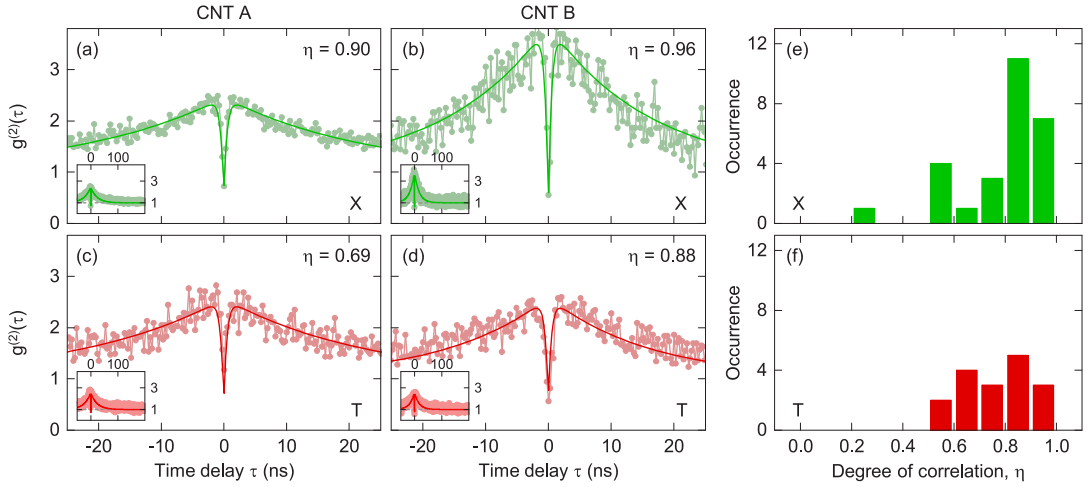

Figure 3. (a–d) Normalized photon coincidence counts $g^{(2)}(\tau)$ in autocorrelation of X (green) and T (red) for two different CNTs A and B, excited resonantly via their respective E_{11} states at 975 and 960 nm with 1 and 3 μW laser power. The insets show $g^{(2)}(\tau)$ on long time scales. The degrees of correlation, $\eta = 1 - g^{(2)}(0)/g^{(2)}_{max}(0)$, given in each graph were obtained from model fits (solid lines) discussed in the main text. (e, f) Degrees of correlation η in autocorrelations of X and T, respectively.

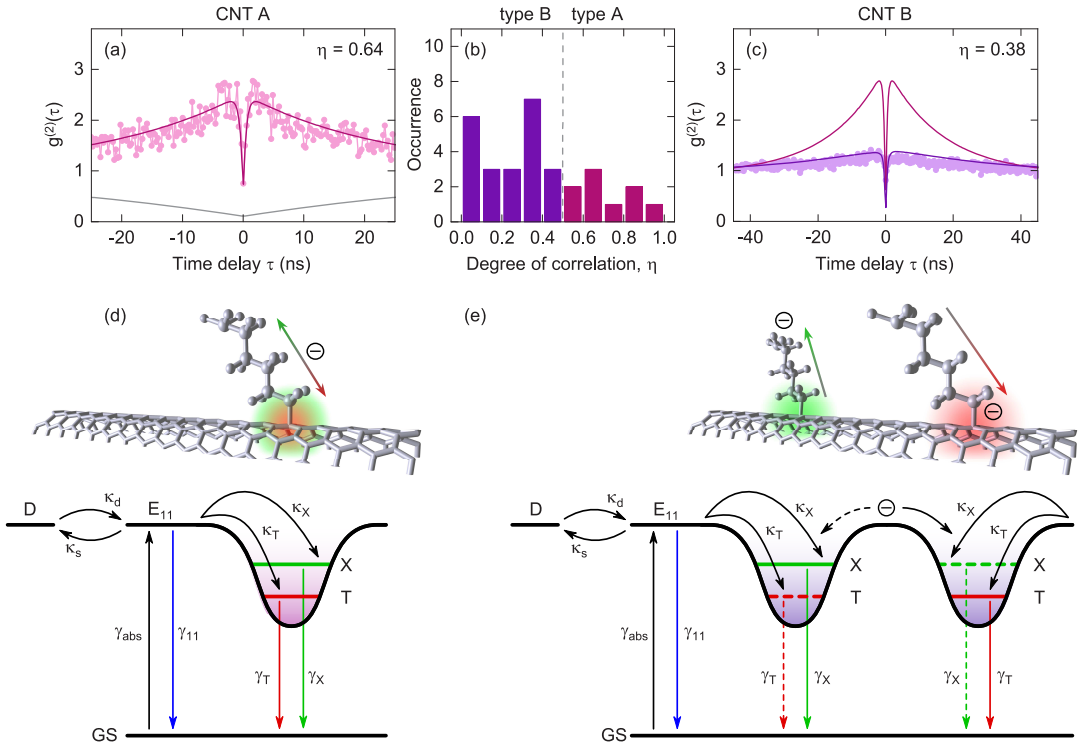

Figure 4. (a, c) Cross-correlations of X and T emission for type A and B nanotubes of Figure 3 excited resonantly via their respective E_{11} states at 975 and 960 nm with 1 and 3 μW laser power. Solid pink and violet lines show predictions according to the models of a single and a double trap state, and the solid gray line shows the prediction of the model of mutually exclusive X and T states without a dark state. (b) Histogram of the degree of correlation in the cross-correlation of X and T. The dashed line at $\eta = 0.5$ separates the CNTs with low (violet) and high degrees of correlation (pink). (d, e) Schematics of defect emission from a single and a double trap state, respectively, corresponding to type A and B nanotubes. The respective level diagrams involve the ground state (GS), exciton continuum (E_{11}), defect-localized states (X, T), and a dark state (D) with model-relevant rates.

was determined as zero within the best-fit error bars, which explains different numbers of closed and open circles in Figure 2d–f for PL decay via E_{11}, X, and T emission, respectively.

Short decay times of E_{11} on time scales below 200 ps are consistent with previous reports for nominally pristine cryogenic nanotubes in linear response,[31] and the two data points in Figure 2d with an additional prolonged decay component with ~200 and 400 ps time constants and weak fractional weights probably reflect some degree of exciton localization in shallow traps of environmental disorder.[8] In contrast, the decay of X and T emission is observed on much longer time scales, with five cases of biexponential decays with comparable fractional weights of the two decay channels (open circles in Figure 2e,f). The prolonged decay times of up to 800 ps are a hallmark of exciton localization in covalently functionalized nanotubes.[32] As the majority of X and T states

DOI: 10.1021/acs.nanolett.9b02553
Nano Lett. 2019, 19, 7078–7084

exhibit simple monoexponential decays of deep exciton-localizing defect potentials, the few contrasting cases of biexponential decays with comparable weights and time scales in Figure 2e,f can be ascribed to two defects, two different CNTs with single-defect sites, or two distinct conformations of a single-defect nanotube. As will become obvious in the following, the signatures of all investigated PL hot-spots were consistent with individual CNTs.

To identify PL hot-spots as stemming from single-tube defects, we performed photon correlation spectroscopy of both X and T luminescent states and studied their mutual correlations. To this end, we used a Hanbury Brown−Twiss (HBT) setup based on two superconducting single-photon detectors in combination with spectral filtering of E_{11}, X, and T emission bands. For autocorrelation measurements, both single-photon detectors were set to detect the PL in the spectral bands of either E_{11}, X or T. In contrast, cross-correlation measurements were performed by selecting different spectral bands in each of the two single-photon counting channels. Figure 3a−d shows normalized coincidence counts $g^{(2)}(\tau)$ recorded in autocorrelation for X (upper panels) and T (lower panels) spectral bands. The autocorrelations of both peaks exhibited antibunching ($g^{(2)}(\tau) < 1$) and bunching ($g^{(2)}(\tau) > 1$) on short and long time scales of 100−700 ps and 10−900 ns, respectively, as characteristic features of intermittent single-photon emission.[9,10,33,34] For sufficiently large delay times, photon emission from both states was uncorrelated, as shown in the insets of Figure 3a−d with $g^{(2)}(\tau)$ approaching unity on long time scales. These signatures establish the sources of PL as single-photon emitters, which we denote as CNTs A and B (with data in the left and right columns of Figure 3a−d, respectively).

To examine the different degrees of antibunching and bunching in autocorrelation measurements of CNT A and B in more detail, we first consider a model of a bright exciton state that exchanges population with a reservoir of dark excitons.[9,33] Within this framework, bunching arises from random transitions to a non-emitting (dark) shelving state and back, and the normalized coincidence function is given by (see Section III of the Supporting Information):

$$g^{(2)}(\tau) = (1 - \eta \times e^{-|\tau|/\tau_{rad}})\left(1 + \frac{\tau_d}{\tau_s} e^{-(\frac{1}{\tau_s}+\frac{1}{\tau_d})|\tau|}\right) \quad (1)$$

where the degree of correlation $\eta = 1 - g^{(2)}(0)/g^{(2)}_{max}(0)$ is defined by the ratio of antibunching to bunching at zero time delay, $g^{(2)}(0)$ and $g^{(2)}_{max}(0) = 1 + \tau_d/\tau_s$, respectively, $\tau_{rad} = 1/\gamma_{rad}$ is the lifetime of the bright exciton with radiative decay rate γ_{rad}, and $\tau_s = 1/\kappa_s$ and $\tau_d = 1/\kappa_d$ are the inverse of shelving and deshelving rates κ_s and κ_d associated with population transfer from the bright to the dark exciton reservoir and back (also indicated in the schematics of Figure 4).

Fitting the autocorrelation data with eq 1, we obtained shelving and deshelving time scales in the range of 10−900 ns (with medians of 37 and 53 ns for τ_s and τ_d) for the X peak and 10−100 ns (with similar medians of 37 and 47 ns for τ_s and τ_d) for the T state emission. The respective histograms of η are shown in Figure 3e,f, where values of η above 0.5 imply strong correlations in the PL emission events of each of the two emissive states X and T as hallmarks of their sub-Poissonian photon emission statistics. In most concise terms, the autocorrelation results of Figure 3e,f identify all X (with one exception with $\eta = 0.25$ in Figure 3e) and T states as blinking single-photon sources.

To relate the PL intermittence of X and T states to their respective exciton population distributions, we first consider the scenario where the two states are their mutual dark reservoirs. Trapping and release of an additional charge at the defect site would switch the nanotube PL between the charged and neutral exciton emission and render X and T the respective dark states of each other, conceptually similar to earlier correlation studies on spectral wandering[9,34] and charge hopping in semiconductor quantum dots.[35−37] In this case, each of the two states would be subjected to blinking and thus exhibit bunching in autocorrelation measurements as in Figure 3. The blinking time scale would then reflect the defect charging dynamics, with the photoexcited population providing snap-shots of a given charge configuration on subnanosecond time scale of radiative decay. This scenario of mutual exclusiveness in X and T emission would imply the absence of a dark reservoir in covalently functionalized CNTs.

The analysis of autocorrelation data of Figure 3 according to this scenario yields a poor quantitative agreement between experiment and model (see also Section III of the Supporting Information). Moreover, it fails to withstand a simple consistency check in cross-correlation measurements of X and T, shown in the upper panel of Figure 4. For the cross-correlation function $g^{(2)}(\tau)$ of Figure 4a, the model of mutually exclusive photon emission events by X and T yields an antibunching dip on the time scale of blinking and no bunching at all (solid gray line in Figure 4a) in agreement with earlier studies of charge-fluctuating quantum emitters.[33−37] The pronounced bunching in the data of Figure 4a, in contrast, signifies that both X and T states blink independently of the defect charge configuration, which is not accounted for by mutually exclusive emission. Moreover, the model requires high degrees of cross-correlation at zero time delay, yet CNTs with $\eta > 0.5$ (pink bars in Figure 4b) were a minority. Instead, most of the CNTs of our study were characterized by weak correlations with $\eta < 0.5$ (violet bars in Figure 4b) in conditioned photon detection events from X and T states. In the following, we assign CNTs with similar signatures in autocorrelation as in Figure 3a−d, yet contrasting degrees of weak and strong cross-correlations in Figure 4b to two disparate classes A and B, respectively.

For both CNT types, the disagreement between the simple model of two mutually exclusive states X and T and the actual observations in cross-correlations can be resolved by introducing an additional dark state. For a single defect site representing type A nanotubes in neutral or charged configuration, the corresponding level diagram of bright E_{11}, X, and T states in the presence of a dark reservoir D is shown in Figure 4d. Although the exciton population in our PL experiments was excited nonresonantly, the excited state can be eliminated by introducing an effective absorption rate γ_{abs} for the generation of E_{11} excitons with radiative decay rate γ_{11}. This photoexcited bright exciton population can either interconvert with the dark reservoir at shelving and deshelving rates κ_s and κ_d or give rise to PL from X and T states at radiative decay rates γ_X and γ_T upon capture at rates κ_X and κ_T by a neutral or charged defect site, respectively. This model yields a set of coupled master equations, which we solve for the temporal evolution of population in the states X and T to obtain the functional dependence for $g^{(2)}(\tau)$ (see Section IV of the Supporting Information for details). Best fits obtained with

DOI: 10.1021/acs.nanolett.9b02553
Nano Lett. 2019, 19, 7078−7084

this model for CNT A are shown as solid green and red lines for the autocorrelation data of X and T in Figure 3a,c and as solid pink line for the X-T cross-correlation data in Figure 4a. We emphasize that all parameters in the fit of cross-correlation results are fixed by the fits to autocorrelation data. The overall good agreement between data and model provides confidence in the scenario for type A tubes shown in Figure 4d.

Despite similarities in autocorrelation, cross-correlations of type B CNTs are not captured by this model (pink line in Figure 4c). It clearly fails to reproduce the data by overestimating both the degree of bunching and antibunching. This observation actually holds for all CNTs with $\eta < 0.5$ in Figure 4b. To interpret the correlation results on this class of CNTs, we assume the presence of two interacting defects within the micron-sized focal spot in our experiment. Each defect would act as a single-photon source within its own spectral band, whereas finite cross-correlations would be ensured by interactions between the proximal defects. This scenario is shown schematically in Figure 4e, where the charge state of the neighboring defects is anticorrelated due to repulsive Coulomb interaction among the excess electrons residing on covalent hexyl chains.[22] In the level diagram of Figure 4e, this is represented by electron hopping between the two defect states.

With this modification, we extended the rate model for type A nanotubes by introducing a second defect site that is favored to be in the opposite charge configuration as its neighbor and again derived $g^{(2)}(\tau)$ by solving the corresponding set of master equations (see Section V of the Supporting Information). While preserving the fit quality for the autocorrelation data of Figure 3b,d, we obtain the violet line in Figure 4c in good agreement with the data. Intuitively, strong autocorrelations paired with weak cross-correlations can be interpreted as follows. By suppressing equal charge configurations of the neighboring defects, antibunching is preserved in autocorrelations of both X and T states since the PL is predominantly emitted in different spectral bands. In cross-correlation measurements, on the other hand, strong correlations are missing due to temporally independent emission from the two defect sites. Interestingly, our analysis of the fit quality also showed that the pronounced bunching in autocorrelations of X and T is reduced in cross-correlation only if the two emissive sites differ in their respective charging and discharging rates.

In summary, we identified both neutral and charged exciton-localizing defect states of hexyl-functionalized (6,5)-CNTs as single-photon sources with strong antibunching in autocorrelations. Complementary cross-correlation measurements provided further insight into the multiplicity of exciton reservoirs that compete for the photoexcited population. In particular, the PL intermittency, manifested by bunching signatures in autocorrelation, can be interpreted quantitatively only on the basis of combined auto- and cross-correlation analysis. As the investigative power of photon cross-correlation spectroscopy is not specific to luminescent quantum defects in CNTs but can be generalized to all quantum emitters with spectral multiplicity, it will prove useful in the search for efficient nonclassical sources based on CNTs[20,38−40] and other materials[3−7,41−44] for future quantum photonic applications.

Methods. Single-chirality (6,5)-CNTs were isolated from CoMoCAT SG65i SWCNTs (lot no. SG65i-L39) using polymer aqueous two-phase extraction.[45] The purified CNTs were stabilized in 1% wt/v sodium dodecyl sulfate (Sigma-Aldrich, >98.5%)-D_2O (Cambridge Isotope Laboratories, Inc., 99.8%), and the CNT solution was diluted to an optical density of 0.1 at E_{11} (988 nm) for subsequent functionalization. The hexyl defects were incorporated into the CNTs by reacting with 1-iodohexane (Sigma-Aldrich, 98%) at a CNT carbon to 1-iodohexane molar ratio of 1:27 in the presence of 7.6 mM of $NaHCO_3$ (EMD chemicals, HPLC grade), 0.16% v/v CH_3CN (Acros organics, HPLC grade, 99.9%), and 3.6 mM of sodium hydrosulfite (Sigma-Aldrich, 85%).[17] The CNT solution was protected from ambient light and stirred with a magnetic stir bar at room temperature for 2 h. The CNT solution was then filtrated through a centrifugal filter (Amicon Ultra-15, MWCO 100 kDa, Sigma-Aldrich) to remove unreacted chemicals and reaction byproduct. The final solution contained individual CNTs that were tailored with hexyl defects and stabilized by 1% wt/v sodium dodecyl sulfate. The solution of functionalized CNTs was characterized by excitation−emission PL spectroscopy (Nanolog spectrometer, Horiba Jobin Yvon).

Samples with dispersed CNTs were prepared by drop-casting out of an aqueous suspension onto the flat side of a hemispherical solid immersion lens (SIL) for PL measurements or onto SiO_2 substrates for inspection with a scanning electron microscope (SEM). The average CNT length of ∼2 μm was determined from SEM measurements. The SIL was placed into the focus of a home-built confocal microscope with slip-stick positioners (attocube systems, ANPxy101 and ANPz102), immersed in a liquid-helium bath cryostat with a base temperature of 4.2 K and excited with a wavelength-tunable Ti:sapphire laser (Coherent, Mira) in continuous wave or pulsed mode. The PL was collected with a low-temperature apochromatic objective (attocube systems, LT-APO/IR/0.81), dispersed by a monochromator (Roper Scientific, Acton SP2500), and recorded with a liquid-nitrogen cooled CCD (Roper Scientific, Spec-10:100BR/LN) or InGaAs array (Roper Scientific, OMA V:1024−1.7 LN). For time-resolved measurements, the PL was excited with the Ti:sapphire laser in pulsed mode and recorded with a superconducting single photon detector (Scontel, TCOPRS-CCR-SW-85). The instrument response function (IRF) was recorded by using an attenuated laser pulse instead of the PL signal. The response of the superconducting single photon detector was time-correlated with the trigger signal from the Ti:sapphire laser by an electronic correlator (PicoQuant, PicoHarp 300). For both auto- and cross-correlation measurements, a second superconducting single photon detector of the same type was used in the HBT setup configuration.

■ ASSOCIATED CONTENT

Supporting Information

The Supporting Information is available free of charge on the ACS Publications website at DOI: 10.1021/acs.nanolett.9b02553.

Additional data as well as details on experimental methods and theoretical modeling (PDF)

■ AUTHOR INFORMATION

Corresponding Author

*E-mail: alexander.hoegele@lmu.de.

ORCID

Mijin Kim: 0000-0002-7781-9466

YuHuang Wang: 0000-0002-5664-1849

Alexander Högele: 0000-0002-0178-9117

DOI: 10.1021/acs.nanolett.9b02553
Nano Lett. 2019, 19, 7078−7084

Notes

The authors declare no competing financial interest.

■ ACKNOWLEDGMENTS

This research was funded by the European Research Council under the ERC grant agreement nos. 336749 and 772195, the Volkswagen Foundation, and the Deutsche Forschungsgemeinschaft (DFG, German Research Foundation) under German Excellence Initiative via the Nanosystems Initiative Munich (NIM) and the Germany's Excellence Strategy - EXC-2111-390814868. A.H. also acknowledges support from the Center for NanoScience (CeNS) and LMUinnovativ. Y.H.W. gratefully acknowledges the National Science Foundation for supporting the Maryland part of work through grant nos. PHY-1839165 and CHE-1507974.

■ REFERENCES

(1) Michler, P.; Kiraz, A.; Becher, C.; Schoenfeld, W. V.; Petroff, P. M.; Zhang, L.; Hu, E.; Imamoglu, A. A Quantum Dot Single-Photon Turnstile Device. *Science* **2000**, *290*, 2282−2285.

(2) Kurtsiefer, C.; Mayer, S.; Zarda, P.; Weinfurter, H. Stable Solid-State Source of Single Photons. *Phys. Rev. Lett.* **2000**, *85*, 290−293.

(3) Tran, T. T.; Bray, K.; Ford, M. J.; Toth, M.; Aharonovich, I. Quantum emission from hexagonal boron nitride monolayers. *Nat. Nanotechnol.* **2016**, *11*, 37−41.

(4) Srivastava, A.; Sidler, M.; Allain, A. V.; Lembke, D. S.; Kis, A.; Imamoğlu, A. Optically active quantum dots in monolayer WSe_2. *Nat. Nanotechnol.* **2015**, *10*, 491−496.

(5) He, Y.-M.; Clark, G.; Schaibley, J. R.; He, Y.; Chen, M.-C.; Wei, Y.-J.; Ding, X.; Zhang, Q.; Yao, W.; Xu, X.; Lu, C.-Y.; Pan, J.-W. Single quantum emitters in monolayer semiconductors. *Nat. Nanotechnol.* **2015**, *10*, 497−502.

(6) Koperski, M.; Nogajewski, K.; Arora, A.; Cherkez, V.; Mallet, P.; Veuillen, J.-Y.; Marcus, J.; Kossacki, P.; Potemski, M. Single photon emitters in exfoliated WSe_2 structures. *Nat. Nanotechnol.* **2015**, *10*, 503−506.

(7) Chakraborty, C.; Kinnischtzke, L.; Goodfellow, K. M.; Beams, R.; Vamivakas, A. N. Voltage-controlled quantum light from an atomically thin semiconductor. *Nat. Nanotechnol.* **2015**, *10*, 507−511.

(8) Högele, A.; Galland, C.; Winger, M.; Imamoğlu, A. Photon Antibunching in the Photoluminescence Spectra of a Single Carbon Nanotube. *Phys. Rev. Lett.* **2008**, *100*, 217401.

(9) Walden-Newman, W.; Sarpkaya, I.; Strauf, S. Quantum Light Signatures and Nanosecond Spectral Diffusion from Cavity-Embedded Carbon Nanotubes. *Nano Lett.* **2012**, *12*, 1934−1941.

(10) Hofmann, M. S.; Glückert, J. T.; Noé, J.; Bourjau, C.; Dehmel, R.; Högele, A. Bright, long-lived and coherent excitons in carbon nanotube quantum dots. *Nat. Nanotechnol.* **2013**, *8*, 502−505.

(11) Sarpkaya, I.; Zhang, Z.; Walden-Newman, W.; Wang, X.; Hone, J.; Wong, C. W.; Strauf, S. Prolonged spontaneous emission and dephasing of localized excitons in air-bridged carbon nanotubes. *Nat. Commun.* **2013**, *4*, 2152.

(12) Ghosh, S.; Bachilo, S. M.; Simonette, R. A.; Beckingham, K. M.; Weisman, R. B. Oxygen Doping Modifies Near-Infrared Band Gaps in Fluorescent Single-Walled Carbon Nanotubes. *Science* **2010**, *330*, 1656−1659.

(13) Piao, Y.; Meany, B.; Powell, L. R.; Valley, N.; Kwon, H.; Schatz, G. C.; Wang, Y. Brightening of carbon nanotube photoluminescence through the incorporation of sp^3 defects. *Nat. Chem.* **2013**, *5*, 840−845.

(14) Miyauchi, Y.; Iwamura, M.; Mouri, S.; Kawazoe, T.; Ohtsu, M.; Matsuda, K. Brightening of excitons in carbon nanotubes on dimensionality modification. *Nat. Photonics* **2013**, *7*, 715−719.

(15) Ma, X.; Adamska, L.; Yamaguchi, H.; Yalcin, S. E.; Tretiak, S.; Doorn, S. K.; Htoon, H. Electronic Structure and Chemical Nature of Oxygen Dopant States in Carbon Nanotubes. *ACS Nano* **2014**, *8*, 10782−10789.

(16) Ma, X.; Hartmann, N. F.; Baldwin, J. K. S.; Doorn, S. K.; Htoon, H. Room-temperature single-photon generation from solitary dopants of carbon nanotubes. *Nat. Nanotechnol.* **2015**, *10*, 671−675.

(17) Kwon, H.; Furmanchuk, A.; Kim, M.; Meany, B.; Guo, Y.; Schatz, G. C.; Wang, Y. Molecularly Tunable Fluorescent Quantum Defects. *J. Am. Chem. Soc.* **2016**, *138*, 6878−6885.

(18) Shiraki, T.; Shiraishi, T.; Juhász, G.; Nakashima, N. Emergence of new red-shifted carbon nanotube photoluminescence based on proximal doped-site design. *Sci. Rep.* **2016**, *6*, 28393.

(19) Maeda, Y.; Minami, S.; Takehana, Y.; Dang, J.-S.; Aota, S.; Matsuda, K.; Miyauchi, Y.; Yamada, M.; Suzuki, M.; Zhao, R.-S.; Zhao, X.; Nagase, S. Tuning of the photoluminescence and up-conversion photoluminescence properties of single-walled carbon nanotubes by chemical functionalization. *Nanoscale* **2016**, *8*, 16916−16921.

(20) He, X.; Hartmann, N. F.; Ma, X.; Kim, Y.; Ihly, R.; Blackburn, J. L.; Gao, W.; Kono, J.; Yomogida, Y.; Hirano, A.; Tanaka, T.; Kataura, H.; Htoon, H.; Doorn, S. K. Tunable room-temperature single-photon emission at telecom wavelengths from sp^3 defects in carbon nanotubes. *Nat. Photonics* **2017**, *11*, 577−582.

(21) He, X.; Gifford, B. J.; Hartmann, N. F.; Ihly, R.; Ma, X.; Kilina, S. V.; Luo, Y.; Shayan, K.; Strauf, S.; Blackburn, J. L.; Tretiak, S.; Doorn, S. K.; Htoon, H. Low-Temperature Single Carbon Nanotube Spectroscopy of sp^3 Quantum Defects. *ACS Nano* **2017**, *11*, 10785−10796.

(22) Kwon, H.; Kim, M.; Nutz, M.; Hartmann, N. F.; Perrin, V.; Meany, B.; Hofmann, M. S.; Clark, C. W.; Doorn, S. K.; Högele, A.; Wang, Y. *Ultra-bright trions observed at fluorescent quantum defects*; submitted for publication.

(23) He, X.; Htoon, H.; Doorn, S. K.; Pernice, W. H. P.; Pyatkov, F.; Krupke, R.; Jeantet, A.; Chassagneux, Y.; Voisin, C. Carbon nanotubes as emerging quantum-light sources. *Nat. Mater.* **2018**, *17*, 663−670.

(24) Brozena, A. H.; Kim, M.; Powell, L. R.; Wang, Y. Controlling the optical properties of carbon nanotubes with organic colour-centre quantum defects. *Nat. Rev. Chem.* **2019**, *3*, 375−392.

(25) Saha, A.; Gifford, B. J.; He, X.; Ao, G.; Zheng, M.; Kataura, H.; Htoon, H.; Kilina, S.; Tretiak, S.; Doorn, S. K. Narrow-band single-photon emission through selective aryl functionalization of zigzag carbon nanotubes. *Nat. Chem.* **2018**, *10*, 1089−1095.

(26) Brozena, A. H.; Leeds, J. D.; Zhang, Y.; Fourkas, J. T.; Wang, Y. Controlled Defects in Semiconducting Carbon Nanotubes Promote Efficient Generation and Luminescence of Trions. *ACS Nano* **2014**, *8*, 4239−4247.

(27) Deng, S.; Zhang, Y.; Brozena, A. H.; Mayes, M. L.; Banerjee, P.; Chiou, W.-A.; Rubloff, G. W.; Schatz, G. C.; Wang, Y. Confined propagation of covalent chemical reactions on single-walled carbon nanotubes. *Nat. Commun.* **2011**, *2*, 382.

(28) Gifford, B. J.; He, X.; Kim, M.; Kwon, H.; Saha, A.; Sifain, A. E.; Wang, Y.; Htoon, H.; Kilina, S.; Doorn, S. K.; Tretiak, S. Optical Effects of Divalent Functionalization of Carbon Nanotubes. *Chem. Mater.* **2019**. DOI: 10.1021/acs.chemmater.9b01438

(29) Gifford, B. J.; Kilina, S.; Htoon, H.; Doorn, S. K.; Tretiak, S. Exciton Localization and Optical Emission in Aryl-Functionalized Carbon Nanotubes. *J. Phys. Chem. C* **2018**, *122*, 1828−1838.

(30) Hofmann, M. S.; Noé, J.; Kneer, A.; Crochet, J. J.; Högele, A. Ubiquity of Exciton Localization in Cryogenic Carbon Nanotubes. *Nano Lett.* **2016**, *16*, 2958−2962.

(31) Hagen, A.; Steiner, M.; Raschke, M. B.; Lienau, C.; Hertel, T.; Qian, H.; Meixner, A. J.; Hartschuh, A. Exponential Decay Lifetimes of Excitons in Individual Single-Walled Carbon Nanotubes. *Phys. Rev. Lett.* **2005**, *95*, 197401.

(32) Hartmann, N. F.; Velizhanin, K. A.; Haroz, E. H.; Kim, M.; Ma, X.; Wang, Y.; Htoon, H.; Doorn, S. K. Photoluminescence Dynamics of Aryl sp^3 Defect States in Single-Walled Carbon Nanotubes. *ACS Nano* **2016**, *10*, 8355−8365.

(33) Santori, C.; Fattal, D.; Vučković, J.; Solomon, G. S.; Waks, E.; Yamamoto, Y. Submicrosecond correlations in photoluminescence from InAs quantum dots. *Phys. Rev. B: Condens. Matter Mater. Phys.* **2004**, *69*, 205324.

DOI: 10.1021/acs.nanolett.9b02553
Nano Lett. 2019, 19, 7078−7084

(34) Sallen, G.; Tribu, A.; Aichele, T.; André, R.; Besombes, L.; Bougerol, C.; Richard, M.; Tatarenko, S.; Kheng, K.; Poizat, J.-P. Subnanosecond spectral diffusion measurement using photon correlation. *Nat. Photonics* **2010**, *4*, 696−699.
(35) Piętka, B.; Suffczyński, J.; Goryca, M.; Kazimierczuk, T.; Golnik, A.; Kossacki, P.; Wysmolek, A.; Gaj, J. A.; Stępniewski, R.; Potemski, M. Photon correlation studies of charge variation in a single GaAlAs quantum dot. *Phys. Rev. B: Condens. Matter Mater. Phys.* **2013**, *87*, 035310.
(36) Chang, W.-H.; Chang, H.-S.; Chen, W.-Y.; Hsu, T. M.; Hsieh, T.-P.; Chyi, J.-I.; Yeh, N.-T. Optical control of the exciton charge states of single quantum dots via impurity levels. *Phys. Rev. B: Condens. Matter Mater. Phys.* **2005**, *72*, 233302.
(37) Shirane, M.; Igarashi, Y.; Ota, Y.; Nomura, M.; Kumagai, N.; Ohkouchi, S.; Kirihara, A.; Ishida, S.; Iwamoto, S.; Yorozu, S.; Arakawa, Y. Charged and neutral biexciton−exciton cascade in a single quantum dot within a photonic bandgap. *Phys. E* **2010**, *42*, 2563−2566.
(38) Khasminskaya, S.; Pyatkov, F.; Słowik, K.; Ferrari, S.; Kahl, O.; Kovalyuk, V.; Rath, P.; Vetter, A.; Hennrich, F.; Kappes, M. M.; Gol'tsman, G.; Korneev, A.; Rockstuhl, C.; Krupke, R.; Pernice, W. H. P. Fully integrated quantum photonic circuit with an electrically driven light source. *Nat. Photonics* **2016**, *10*, 727−732.
(39) Jeantet, A.; Chassagneux, Y.; Claude, T.; Roussignol, P.; Lauret, J. S.; Reichel, J.; Voisin, C. Exploiting One-Dimensional Exciton−Phonon Coupling for Tunable and Efficient Single-Photon Generation with a Carbon Nanotube. *Nano Lett.* **2017**, *17*, 4184−4188.
(40) Luo, Y.; Ahmadi, E. D.; Shayan, K.; Ma, Y.; Mistry, K. S.; Zhang, C.; Hone, J.; Blackburn, J. L.; Strauf, S. Purcell-enhanced quantum yield from carbon nanotube excitons coupled to plasmonic nanocavities. *Nat. Commun.* **2017**, *8*, 1413.
(41) Kolesov, R.; Xia, K.; Reuter, R.; Stöhr, R.; Zappe, A.; Meijer, J.; Hemmer, P. R.; Wrachtrup, J. Optical detection of a single rare-earth ion in a crystal. *Nat. Commun.* **2012**, *3*, 1029.
(42) Aharonovich, I.; Neu, E. Diamond Nanophotonics. *Adv. Opt. Mater.* **2014**, *2*, 911−928.
(43) Morfa, A. J.; Gibson, B. C.; Karg, M.; Karle, T. J.; Greentree, A. D.; Mulvaney, P.; Tomljenovic-Hanic, S. Single-Photon Emission and Quantum Characterization of Zinc Oxide Defects. *Nano Lett.* **2012**, *12*, 949−954.
(44) Castelletto, S.; Johnson, B. C.; Ivády, V.; Stavrias, N.; Umeda, T.; Gali, A.; Ohshima, T. A silicon carbide room-temperature single-photon source. *Nat. Mater.* **2014**, *13*, 151−156.
(45) Ao, G.; Streit, J. K.; Fagan, J. A.; Zheng, M. Differentiating Left- and Right-Handed Carbon Nanotubes by DNA. *J. Am. Chem. Soc.* **2016**, *138*, 16677−16685.

DOI: 10.1021/acs.nanolett.9b02553
Nano Lett. 2019, 19, 7078−7084